Published in IET Power Electronics
Received on 31st July 2009
Revised on 6th January 2010
doi: 10.1049/iet-pel.2009.0289

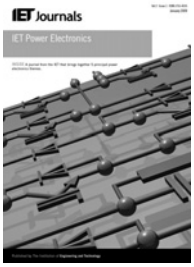

ISSN 1755-4535

Winding losses caused by harmonics in high-frequency flyback transformers for pulse-width modulated dc–dc converters in discontinuous conduction mode

D. Murthy-Bellur M.K. Kazimierczuk

Department of Electrical Engineering, Wright State University, OH 45435, USA
E-mail: murthybellur.2@wright.edu

Abstract: High-frequency transformers used in pulse-width modulated (PWM) converters conduct periodic non-sinusoidal currents, which give rise to additional winding losses because of harmonics. This study presents expressions for winding power losses in a two-winding transformer subject to non-sinusoidal excitation operated in discontinuous conduction mode (DCM). Dowell's equation is used to determine the winding resistances because of eddy currents as a function of frequency. Both skin and proximity effects are taken into account. Fourier series of the primary and secondary triangular current waveforms in isolated dc–dc power converters and the primary and secondary winding resistances are used to determine the primary and secondary winding power losses at various harmonics, respectively. The harmonic winding loss factors F_{Rph} and F_{Rsh} are introduced. The theory is illustrated by the case study of the two-winding flyback converter operating in DCM. Plots of the winding power losses are given as functions of the output power and the dc input voltage.

1 Introduction

Magnetic components such as inductors and transformers are an integral part of modern power electronic equipments. They occupy more volume and are heavier when compared to other parts in a power electronic converter. In order to reduce the size of the magnetic components, the switching frequency of the pulse-width modulated (PWM) converters is increased. Increasing the switching frequency of the converter increases the transformer winding losses because of skin and proximity effects. Additionally, since PWM converters conduct periodic non-sinusoidal currents in steady state, the losses because of harmonics increase the winding power losses. The harmonic losses in transformer windings because of high-frequency (HF) operation also increase the operating temperature. HF transformers are widely used in power-factor correction and dc–dc power conversion applications [1–5].

The effect of HF operation in windings and cores is studied in many papers [6–32]. The winding ac resistance caused by the skin and proximity effects for sinusoidal current in a winding is studied in [6–8]. The theoretical analyses presented in [6–8] are further extended in [9–15]. In another recently proposed method [16], the rms values of the current waveform and the rms value of its derivatives are used to find the ac resistance for a number of arbitrary waveforms. A procedure to design transformers for PWM dc–dc converters is available in [33]. However, the transformer design in [33] neither calculates the winding losses because of HF effects nor because of harmonics. The Fourier expansion of the flyback transformer primary and secondary triangular current waveforms in PWM converters operating in discontinuous conduction mode (DCM) as shown in Fig. 1 has not been given in the literature.

The objectives of the paper are: (i) to develop winding power loss equations of a two-winding transformer conducting periodic non-sinusoidal triangular currents with harmonics such as in flyback PWM converters in DCM, using Dowell's theory, (ii) to give a step-by-step procedure and an example to design a transformer, using the area

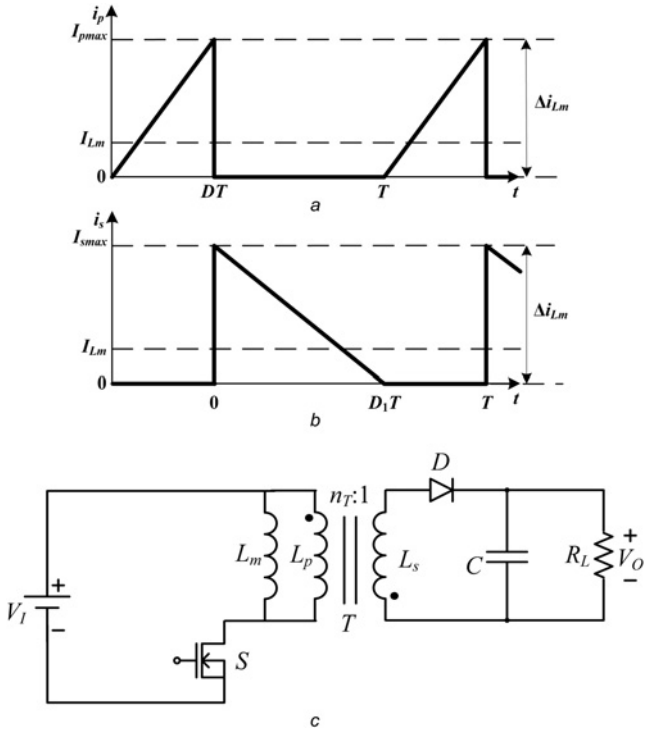

Figure 1 *Two-winding flyback transformer current waveforms for DCM and flyback converter circuit*

a Primary winding current i_p
b Secondary winding current i_s
c Flyback PWM dc–dc converter circuit

product method, and (iii) to study the effect of winding losses on the behaviour of a flyback PWM dc–dc converter in DCM over the entire range of converter operation.

Sections 2 and 3 present the derivation of core area product and winding power loss equations for periodic non-sinusoidal transformer current waveforms for DCM, respectively. The procedure to design a two-winding transformer for a flyback PWM dc–dc converter operated in DCM is given in Section 4. In Section 5, flyback DCM transformer characteristic charts are shown. Finally, in Section 6, conclusions and discussions are presented.

2 Core area product for a two-winding flyback transformer

The magnetic flux linkage (magnetic flux ϕ linking N_p turns of the primary winding of the transformer) is given by

$$\lambda(t) = N_p\phi(t) = N_pA_cB(t) = L_pi_p(t) \tag{1}$$

where A_c is the core cross-sectional area in m^2 and B is the magnetic flux density in T. For the peak values, this equation becomes

$$\lambda_{pk} = N_p\phi_{pk} = N_pA_cB_{pk} = L_pI_{pmax} \tag{2}$$

The maximum current density of the primary winding wire is

$$J_m = \frac{I_{pmax}}{A_{wp}} \tag{3}$$

where A_{wp} is the primary winding bare wire cross-sectional area in m^2. The window area limited by the maximum current density in the winding wire is given by

$$W_a = \frac{N_pA_{wp} + N_sA_{ws}}{K_u} \tag{4}$$

where N_s is the number of turns of the secondary winding and A_{ws} is the secondary winding bare wire cross-sectional area in m^2. Assuming the winding allocation is such that $N_pA_{wp} = N_sA_{ws}$, the window area is

$$W_a = \frac{2N_pA_{wp}}{K_u} \tag{5}$$

where the window utilisation factor is defined as

$$K_u = \frac{A_{Cu}}{W_a} = \frac{2N_pA_{wp}}{W_a} \tag{6}$$

where A_{Cu} is the total copper area in the window in m^2. The maximum energy stored in the magnetic field of the transformer is $W_m = (1/2)L_mI^2_{Lm(max)}$, where L_m and I_{Lm} are the transformer magnetising inductance and magnetising current amplitude, respectively. Assuming that $L_p \simeq L_m$ and $I_{pmax} \simeq I_{Lm(max)}$, and using (2), (3) and (5), the area product of the core is defined as

$$A_p = W_aA_c = \frac{2L_pI^2_{pmax}}{K_uJ_mB_{pk}} = \frac{4W_m}{K_uJ_mB_{pk}} \tag{7}$$

The parameter A_p in (7) is also called the ferrite-copper area product. The value of A_p can be decreased by increasing the values of K_u, J_m and $B_{pk} < B_s$, where B_s is the core saturation flux density. Equation (7) gives a measure of energy handling capability of a core and can be used to select a suitable core using the manufacturer's datasheets.

3 Copper power loss in transformer for periodic non-sinusoidal current waveforms for DCM

3.1 Transformer primary winding power loss

The current waveform of the transformer primary winding for DCM in steady state is shown in Fig. 1*a* and is given by

$$i_p = \begin{cases} \dfrac{I_{pmax}t}{DT} & \text{for } 0 < t \le DT \\ 0 & \text{for } DT < t \le T \end{cases} \tag{8}$$

The dc component of the primary winding current waveform for DCM is

$$I_{\mathrm{pdc}} = \frac{1}{T}\int_0^T i_{\mathrm{p}}\,\mathrm{d}t = \frac{I_{\mathrm{pmax}}}{DT^2}\int_0^{DT} t\,\mathrm{d}t = \frac{DI_{\mathrm{pmax}}}{2} \tag{9}$$

The Fourier series coefficients of the primary current waveform are

$$a_n = \frac{2}{T}\int_0^T i_{\mathrm{p}}\cos(n\omega t)\,\mathrm{d}t = \frac{2I_{\mathrm{pmax}}}{DT^2}\int_0^{DT} t\cos(n\omega t)\,\mathrm{d}t$$
$$= \frac{I_{\mathrm{pmax}}}{2\pi^2 n^2 D}[\cos(2\pi nD) - 1 + 2\pi nD\sin(2\pi nD)] \tag{10}$$

and

$$b_n = \frac{2}{T}\int_0^T i_{\mathrm{p}}\sin(n\omega t)\,\mathrm{d}t = \frac{2I_{\mathrm{pmax}}}{DT^2}\int_0^{DT} t\sin(n\omega t)\,\mathrm{d}t$$
$$= \frac{I_{\mathrm{pmax}}}{2\pi^2 n^2 D}[\sin(2\pi nD) - 2\pi nD\cos(2\pi nD)] \tag{11}$$

which gives the amplitudes of the fundamental component and the harmonics of the primary winding current waveform

$$I_{\mathrm{p}n} = \sqrt{a_n^2 + b_n^2} = \frac{I_{\mathrm{pmax}}}{2\pi^2 n^2 D} \times \sqrt{2[1 + 2\pi^2 n^2 D^2 - 2n\pi\sin(2\pi nD) - \cos 2\pi nD]}$$
$$= \frac{I_{\mathrm{pdc}}}{\pi^2 n^2 D^2} \times \sqrt{2[1 + 2\pi^2 n^2 D^2 - 2n\pi\sin(2\pi nD) - \cos 2\pi nD]} \tag{12}$$

The power loss in the primary winding is

$$P_{\mathrm{wp}} = R_{\mathrm{wpdc}} I_{\mathrm{pdc}}^2\left[1 + \frac{1}{2}\sum_{n=1}^{\infty}\left(\frac{R_{\mathrm{wpn}}}{R_{\mathrm{wpdc}}}\right)\left(\frac{I_{\mathrm{pn}}}{I_{\mathrm{pdc}}}\right)^2\right]$$
$$= P_{\mathrm{wpdc}}\left[1 + \frac{1}{2}\sum_{n=1}^{\infty} F_{\mathrm{Rpn}}\left(\frac{I_{\mathrm{pn}}}{I_{\mathrm{pdc}}}\right)^2\right]$$
$$= P_{\mathrm{wpdc}}\left\{1 + \frac{1}{\pi^4 D^4}\sum_{n=1}^{\infty}\frac{F_{\mathrm{Rpn}}}{n^4}[1 + 2\pi^4 n^2 D^2 - \cos(2\pi nD) - 2\pi nD\sin(2\pi nD)]\right\}$$
$$= P_{\mathrm{wpdc}} F_{\mathrm{Rpn}} \tag{13}$$

The primary winding ac-to-dc resistance ratio at the fundamental frequency and harmonic frequencies is

$$F_{\mathrm{Rpn}} = \frac{R_{\mathrm{wp}n}}{R_{\mathrm{wpdc}}} = A\sqrt{n}\left\{\frac{\sinh(2A\sqrt{n}) + \sin(2A\sqrt{n})}{\cosh(2A\sqrt{n}) - \cos(2A\sqrt{n})} + \left[\frac{2(N_{\mathrm{l}}^2 - 1)}{3}\right]\frac{\sinh(A\sqrt{n}) + \sin(A\sqrt{n})}{\cosh(A\sqrt{n}) - \cos(A\sqrt{n})}\right\} \tag{14}$$

where N_{l} is the number of layers of the primary winding and A is the winding conductor thickness normalised with respect to the conductor skin depth at the switching frequency. The factor F_{Rpn} takes into account the skin and proximity effect in the winding. The derivation of ac resistance factor F_{R} is obtained from Dowell's one-dimensional solution [7] and is

$$F_{\mathrm{R}} = \frac{R_{\mathrm{w}}}{R_{\mathrm{wpdc}}} = F_{\mathrm{S}} + F_{\mathrm{P}} = A\left\{\frac{\sinh(2A) + \sin(2A)}{\cosh(2A) - \cos(2A)} + \left[\frac{2(N_{\mathrm{l}}^2 - 1)}{3}\right]\frac{\sinh(A) + \sin(A)}{\cosh(A) - \cos(A)}\right\} \tag{14a}$$

In (14*a*), the first term represents the winding ac resistance because of skin effect F_{S} and the second term the winding ac resistance because of proximity effect F_{P}. Notice that F_{Rpn} and F_{R} are different as the former is dependent on harmonics. The primary winding harmonic loss factor is defined as the total primary winding dc and the primary winding ac power loss normalised with respect to the primary winding dc power loss given by

$$F_{\mathrm{Rph}} = \frac{P_{\mathrm{wp}}}{P_{\mathrm{wpdc}}} = 1 + \frac{1}{2}\sum_{n=1}^{\infty} F_{\mathrm{Rpn}}\left(\frac{I_{\mathrm{pn}}}{I_{\mathrm{pdc}}}\right)^2$$
$$= 1 + \frac{1}{\pi^4 D^4}\sum_{n=1}^{\infty}\frac{F_{\mathrm{Rpn}}}{n^4} \times [1 + 2\pi^2 n^2 D^2 - \cos(2\pi nD) - 2\pi nD\sin(2\pi nD)] \tag{15}$$

The skin depth of the winding conductor at the nth harmonic is

$$\delta_{wn} = \frac{\delta_{w1}}{\sqrt{n}} \tag{16}$$

where δ_{w1} is the conductor skin depth at the fundamental frequency. The winding conductor thickness normalised with respect to the conductor skin depth is

$$A_n = \frac{h}{\delta_{wn}} = \frac{h\sqrt{n}}{\delta_{w1}} = A\sqrt{n} \tag{17}$$

For a rectangular conductor, A is given by

$$A = \frac{h}{\delta_{w1}}\sqrt{\frac{w}{p}} \tag{18}$$

doi: 10.1049/iet-pel.2009.0289

For a square conductor, A is given by

$$A = \frac{h}{\delta_{w1}}\sqrt{\frac{h}{p}} \tag{19}$$

For a round conductor, A is given by

$$A = \left(\frac{\pi}{4}\right)^{3/4}\frac{d}{\delta_{w1}}\sqrt{\frac{d}{p}} \tag{20}$$

In (18), (19) and (20), w/p, h/p and d/p are called the layer porosity factors, w is the width of the rectangular bare conductor, h is the thickness of the square and rectangular bare conductors, d is the diameter of the round bare conductor and p is the distance between the centres of two adjacent conductors, called the winding pitch.

3.2 Transformer secondary winding power loss

The current waveform of the transformer secondary winding for DCM in steady state is shown in Fig. 1*b* and is given by

$$i_s = \begin{cases} -\dfrac{I_{\text{smax}}t}{D_1T} + I_{\text{smax}} & \text{for } 0 < t \le D_1T \\ 0, & \text{for } D_1T < t \le T \end{cases} \tag{21}$$

The dc component of the secondary winding current waveform for DCM is

$$I_{\text{sdc}} = \frac{1}{T}\int_0^T i_s\,\mathrm{d}t = \frac{I_{\text{smax}}}{T}\int_0^{D_1T}\left(1 - \frac{t}{D_1T}\right)\mathrm{d}t = \frac{D_1I_{\text{smax}}}{2} \tag{22}$$

The Fourier series coefficients of the secondary current

Table 1 Two-winding transformer design for flyback PWM DC-DC converter in DCM

Step number	Parameter	Equation	Value
1	input voltage	V_{I}	100 $\pm$ 20 V
2	output voltage	V_{O}	48 V
3	switching frequency	f_{s}	100 kHz
4	output power	P_{O}	60 W
5	dc voltage transfer function	M_{VDC}	
5a		$M_{\text{VDC min}} = \dfrac{V_{\text{O}}}{V_{\text{Imax}}}$	0.4
5b		$M_{\text{VDCmax}} = \dfrac{V_{\text{O}}}{V_{\text{Imin}}}$	0.6
6	transformer primary-to-secondary turns ratio†	$n_T = \dfrac{\eta D_{\text{max}}}{(1 - D_{\text{max}})M_{\text{VDCmax}}}$	1.466
7	maximum magnetising inductance for DCM	$L_{\text{p}} \simeq L_{\text{m(max)}} = \dfrac{n_T^2R_{\text{Lmin}}(1 - D_{\text{max}})^2}{2f_s}$	103.16 µH pick 82 µH
8	secondary winding inductance	$L_{\text{s}} = \dfrac{L_p}{n_T^2}$	38.15 µH
9	maximum duty cycle	$D_{\text{max}} = M_{\text{VDCmax}}\sqrt{\dfrac{2f_{\text{s}}L_{\text{m}}}{\eta R_{\text{Lmin}}}}$	0.418
10	minimum duty cycle	$D_{\text{min}} = M_{\text{VDCmin}}\sqrt{\dfrac{2f_{\text{s}}L_{\text{m}}}{\eta R_{\text{Lmin}}}}$	0.2786
11	maximum duty cycle when the diode is ON	$D_{1\,\text{max}} = \sqrt{\dfrac{2f_{\text{s}}L_{\text{m}}}{n_T^2R_{\text{Lmin}}}}$	0.4457

Continued

Table 1 *Continued*

Step number	Parameter	Equation	Value
12	maximum dc input current	$I_{\text{Imax}} = \frac{M_{\text{VDCmax}} I_{\text{Omax}}}{\eta}$	0.8523 A
13	maximum peak primary winding current	$I_{\text{pmax}} = \Delta i_{\text{Lm(max)}} = \frac{D_{\min} V_{\text{Imax}}}{f_s L_p}$	4.077 A
14	maximum primary rms current	$I_{\text{prms(max)}} = I_{\text{pmax}} \sqrt{\frac{D_{\max}}{3}}$	1.521 A
15	window utilisation factor	K_u	0.3
16	peak flux density	B_{pk}	0.25
17	maximum current density of the winding wire	J_m	5 A/mm^2
18	maximum energy stored in the transformer magnetic field	$W_m = \frac{1}{2} L_p I_{\text{pmax}}^2$	0.681 mJ
19	core area product (calculated)	$A_p = W_a A_c = \frac{4 W_m}{K_u J_m B_{\text{pk}}}$	0.7264 cm^4
20	selected core	magnetics ferrite p-type pot core	0P-43019
21	core area product of the selected core	A_p	0.73 cm^4
22	core cross-sectional area	A_c	1.37 cm^2
23	core window area	W_a	0.5328 cm^2
24	mean magnetic path length (MPL)	l_c	4.52 cm
25	mean length of single turn	l_T	6.078 cm
26	core volume	V_c	6.19 cm^3
27	core permeability	μ_{rc}	2500 $\pm$ 25%
28	core saturation flux density	B_s	0.49 T
29	core power loss density coefficients (for P-type ferrite material and 100 kHz $\leq f_s <$ 500 kHz)		
29(a)		k	0.0434
29(b)		a	1.63
29(c)		b	2.62
30	skin depth of copper wire (at 20°C and $f_s = 100$ kHz)	$\delta_{w1} = \frac{\sqrt{\rho_{\text{Cu(20°C)}}}}{\pi f_s \mu_0}$	0.209 mm
31	selected copper wire	AWG	no. 26
32	bare wire diameter of the strand wire	d_{is}	0.405 mm
33	insulated wire diameter of the strand wire	d_{os}	0.452 mm
34	bare wire cross-section area of the strand	A_{wsi}	0.1288 mm^2
35	insulated wire cross-section area of the strand	A_{wso}	0.1604 mm^2
36	dc resistance of the strand per unit length	R_{wdc}/l_w	0.1345 Ω/m

Continued

IET Power Electron., 2010, Vol. 3, Iss. 5, pp. 804–817

doi: 10.1049/iet-pel.2009.0289

Table 1 *Continued*

Step number	Parameter	Equation	Value
37	cross-sectional area of the primary winding wire	$A_{wp} = \frac{I_{pmax}}{J_m}$	0.8154 mm^2
38	number of strands in the primary winding	$S_p = \frac{A_{wp}}{A_{wsi}}$	6.33 pick 6
39	number of turns of the primary winding	$N_p = \frac{K_u(W_a/2)}{S_p A_{wsi}}$	10.34 pick 10
40	number of turns of the secondary winding	$N_s = \frac{N_p}{n_T}$	6.82 pick 7
41	air gap length	$l_g = \frac{\mu_0 A_c N_p^2}{L_p} - \frac{l_c}{\mu_{rc}}$	0.191 mm
42(a)	maximum peak magnetic flux density	$B_{pk} = \frac{\mu_0 N_p I_{pmax}}{l_g + (l_c/\mu_{rc})}$	0.245 T
42(b)	maximum magnetic flux density ac component	$B_m = \frac{B_{pk}}{2}$	0.1225 T
43	core power loss density	$P_v = k(f_s \text{ in kHz})^a(10B_m)^b$	134.4 mW/cm^3
44	core loss	$P_c = V_c P_v$	0.832 W
45	total length of the primary winding wire	$l_{wp} = N_p l_T$	60.78 cm pick 65 cm
46	primary strand dc and low-frequency resistance	$R_{wpdcs} = \left(\frac{R_{wdc}}{l_w}\right) l_{wp}$	0.0874 Ω
47	primary winding dc and low-frequency resistance	$R_{wpdc} = \frac{R_{wpdcs}}{S_p}$	14.57 mΩ
48	primary winding dc and low-frequency power loss	$P_{wpdc} = R_{wpdc} I_{lmax}^2$	0.01058 W
49	primary winding harmonic loss factor	F_{Rph} (use (15) @ V_{lmin}, P_{Omax})	11.95
50	primary winding total power loss	$P_{wp} = F_{Rph} P_{wpdc}$	0.1264 W
51	maximum peak secondary winding current	$I_{smax} = n_T \Delta i_{Lm(max)}$	5.97 A
52	maximum secondary rms current	$I_{srms(max)} = I_{smax}\sqrt{\frac{D_{1\,max}}{3}}$	2.3 A
53	cross-sectional area of the secondary winding wire	$A_{ws} = \frac{I_{smax}}{J_m}$	1.194 mm^2
54	number of strands in the secondary winding	$S_s = \frac{A_{ws}}{A_{wsi}}$	9.27 Pick 9
55	total length of the secondary winding wire	$l_{ws} = N_s l_T$	42.54 cm Pick 47 cm
56	secondary strand dc and low-frequency resistance	$R_{wsdcs} = \left(\frac{R_{wdc}}{l_w}\right) l_{ws}$	0.0632 Ω

Continued

Table 1 *Continued*

Step number	Parameter	Equation	Value
57	secondary winding dc and low-frequency resistance	$R_{wsdc} = \left(\frac{R_{wsdcs}}{S_s}\right)$	7.02 mΩ
58	secondary winding dc and low-frequency power loss	$P_{wsdc} = R_{wsdc} I_{Omax}^2$	0.01096 W
59	secondary winding harmonic loss factor	F_{Rsh} (use (27) @ P_{Omax})	4.86
60	secondary winding total power loss	$P_{ws} = F_{Rsh} P_{wsdc}$	0.0532 W
61	DC and low-frequency power loss in both windings	$P_{wdc} = P_{wpdc} + P_{wsdc}$	0.02154 W
62	total winding power loss	$P_w = P_{wp} + P_{ws}$	0.1796 W
63	total transformer power loss	$P_{cw} = P_c + P_w$	1.011 W
64	total core surface area	A_t	31.95 cm^2
65	surface power loss density	$\psi = \frac{P_{cw}}{A_t}$	0.0316 W/cm^2
65	temperature rise of the transformer	$\Delta T = 450\psi^{0.826}$	25.94°C
67	window utilisation factor (recalculated)	$K_u = \frac{(N_p S_p + N_s S_s) A_{wst}}{W_a}$	0.2973
68	transformer efficiency at full power	$\eta_t = \frac{P_O}{P_O + P_{cw}}$	98.34%

[†]Assume converter efficiency $\eta = 0.88$ and $D_{max} = 0.5$

waveform are

$$a_n = \frac{2}{T}\int_0^T i_s \cos(n\omega t)\,dt = \frac{2I_{smax}}{T} \times \int_0^{D_1 T}\left(1 - \frac{t}{D_1 T}\right)\cos(n\omega t)\,dt = \frac{I_{smax}}{2\pi^2 n^2 D_1}[1 - \cos(2\pi n D_1)] \quad (23)$$

and

$$b_n = \frac{2}{T}\int_0^T i_s \sin(n\omega t)\,dt = \frac{2I_{smax}}{T} \times \int_0^{D_1 T}\left(1 - \frac{t}{D_1 T}\right)\sin(n\omega t)\,dt = \frac{I_{smax}}{2\pi^2 n^2 D_1}[2\pi n D_1 - \sin(2\pi n D_1)] \quad (24)$$

yielding the amplitudes of the fundamental component and the harmonics of the secondary winding current waveform

$$I_{sn} = \sqrt{a_n^2 + b_n^2} = \frac{I_{smax}}{2\pi^2 n^2 D_1} \times \sqrt{2\{1 - \cos(2\pi n D_1) + 2\pi n D_1[\pi n D_1 - \sin(2\pi n D_1)]\}} = \frac{I_{sdc}}{\pi^2 n^2 D_1^2} \times \sqrt{2\{1 - \cos(2\pi n D_1) + 2\pi n D_1[\pi n D_1 - \sin(2\pi n D_1)]\}} \quad (25)$$

The power loss in the secondary winding is

$$\begin{aligned} P_{ws} &= R_{wsdc} I_{sdc}^2 \left[1 + \frac{1}{2}\sum_{n=1}^{\infty}\left(\frac{R_{wsn}}{R_{wsdc}}\right)\left(\frac{I_{sn}}{I_{sdc}}\right)^2\right] \\ &= P_{wsdc}\left[1 + \frac{1}{2}\sum_{n=1}^{\infty} F_{Rsn}\left(\frac{I_{sn}}{I_{sdc}}\right)^2\right] \\ &= P_{wsdc} + \left\langle 1 + \frac{1}{\pi^4 D_1^4}\sum_{n=1}^{\infty}\frac{F_{Rsn}}{n^4}\{1 - \cos(2\pi n D_1) + 2\pi n D_1[\pi n D_1 - \sin(2\pi n D_1)]\}\right\rangle \\ &= P_{wsdc} F_{Rsn} \end{aligned} \quad (26)$$

The relationship between D and D_1 is converter dependent. The secondary winding harmonic loss factor is defined as the total secondary winding dc and the secondary winding ac power loss normalised with respect to the secondary

IET Power Electron., 2010, Vol. 3, Iss. 5, pp. 804–817
doi: 10.1049/iet-pel.2009.0289

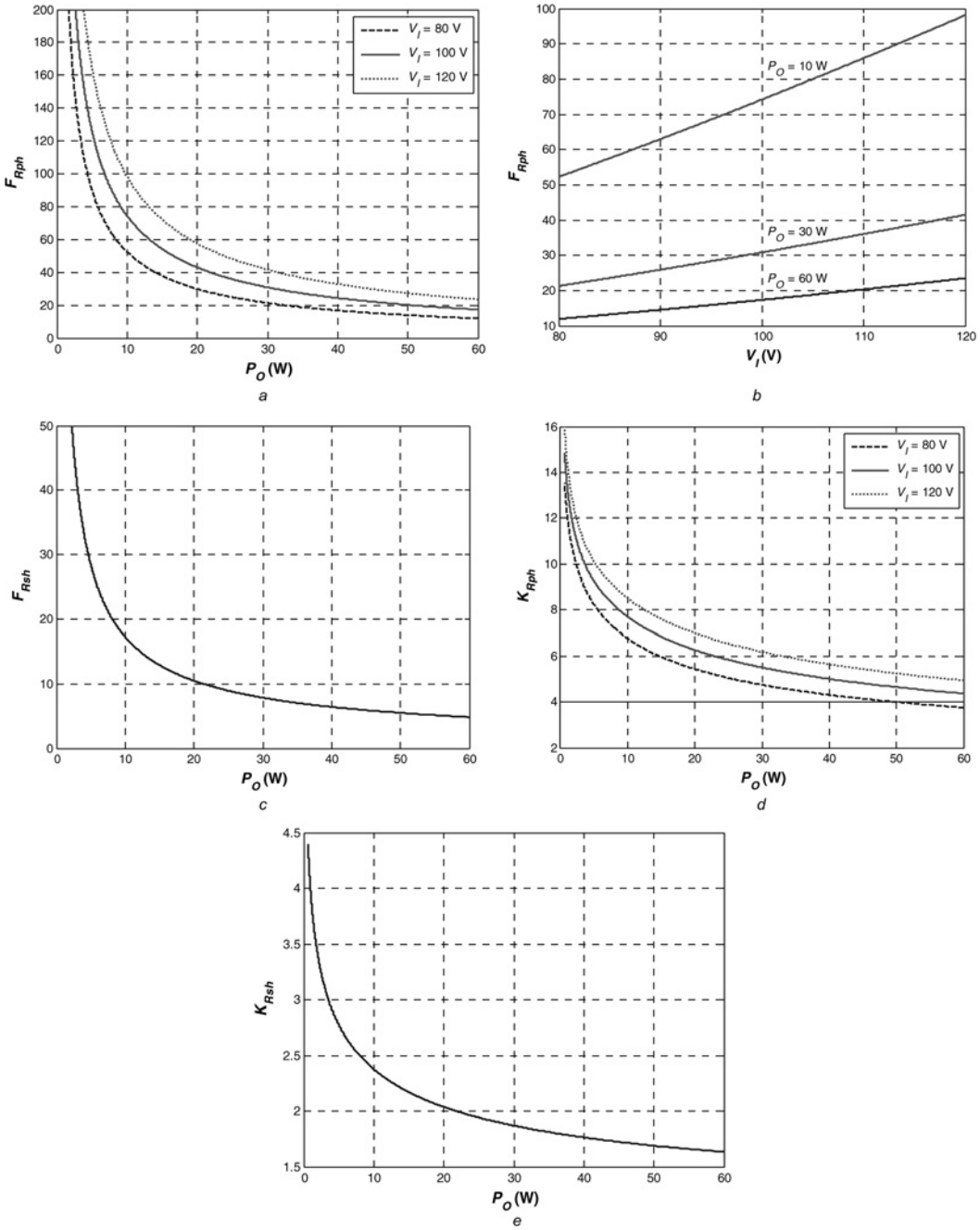

Figure 2 *Winding harmonic loss factors*

a Primary winding harmonic loss factor F_{Rph} as a function of the output power P_O at fixed values of the dc input voltage V_I
b Primary winding harmonic loss factor F_{Rph} as a function of the dc input voltage V_I at fixed values of the output power P_O
c Secondary winding harmonic loss factor F_{Rsh} as a function of the output power P_O
d Effective primary winding resistance factor K_{Rph} as a function of the output power P_O at fixed values of the DC input voltage V_I
e Effective secondary winding resistance factor K_{Rsh} as a function of the output power P_O.

winding dc power loss given by

$$F_{\mathrm{Rsh}} = \frac{P_{\mathrm{ws}}}{P_{\mathrm{wsdc}}} = 1 + \frac{1}{2}\sum_{n=1}^{\infty} F_{\mathrm{Rsn}}\left(\frac{I_{\mathrm{sn}}}{I_{\mathrm{sdc}}}\right)^2$$
$$= 1 + \frac{1}{\pi^4 D_1^4}\sum_{n=1}^{\infty}\frac{F_{\mathrm{Rsn}}}{n^4}\{1 - \cos(2\pi n D_1) + 2\pi n D_1$$
$$\times [\pi n D_1 - \sin(2\pi n D_1)]\} \quad (27)$$

In (27), F_{Rsn} can be computed using (14), by considering N_I of the secondary winding, and using (18), (19) and (20) for rectangular, square or round secondary winding wire, respectively.

3.3 Effective primary and secondary winding resistance factors

The total primary winding power loss, because of both dc and all harmonics, can be expressed in terms of the effective

Table 2 Variation of F_{Rph} and F_{Rsh} with respect to the number of harmonics at $P_{O(max)}$ and $V_{I(max)}$

Number of harmonics n	Primary winding harmonic loss factor F_{Rph}	Secondary winding harmonic loss factor F_{Rsh}
1	5.33	2.71
2	10.66	3.32
3	13.66	3.56
5	15.86	3.89
10	18.79	4.25
25	21.28	4.57
50	22.58	4.74
100	23.51	4.86
200	24.17	4.95
500	24.72	5.03

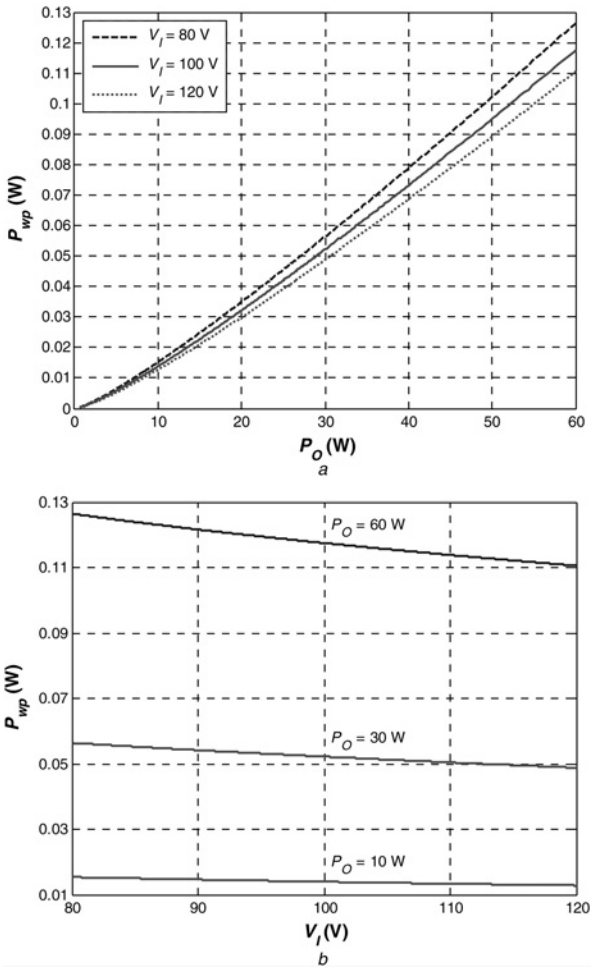

Figure 3 *Primary winding loss*

a Primary winding loss P_{wp} as a function of the output power P_O at fixed values of the dc input voltage V_I

b Primary winding loss P_{wp} as a function of the dc input voltage V_I at fixed values of the output power P_O

primary winding resistance R_{wpe} as

$$P_{wp} = R_{wpe} I^2_{p(rms)} = R_{wpdc} I^2_{pdc} \left[1 + \frac{1}{2} \sum_{n=1}^{\infty} \left(\frac{I_{pn}}{I_{pdc}} \right)^2 \right] \quad (28)$$

Equating (13) to (28), one obtains the effective primary winding resistance factor

$$K_{Rph} = \frac{R_{wpe}}{R_{wpdc}} = \frac{1 + (1/2) \sum_{n=1}^{\infty} F_{Rpn} (I_{pn}/I_{pdc})^2}{1 + (1/2) \sum_{n=1}^{\infty} (I_{pn}/I_{pdc})^2} = \frac{F_{Rph}}{1 + (1/2) \sum_{n=1}^{\infty} (I_{pn}/I_{pdc})^2} \quad (29)$$

resulting in the total primary winding power loss

$$P_{wp} = R_{wpe} I^2_{p(rms)} = K_{Rph} R_{wpdc} I^2_{p(rms)} \quad (30)$$

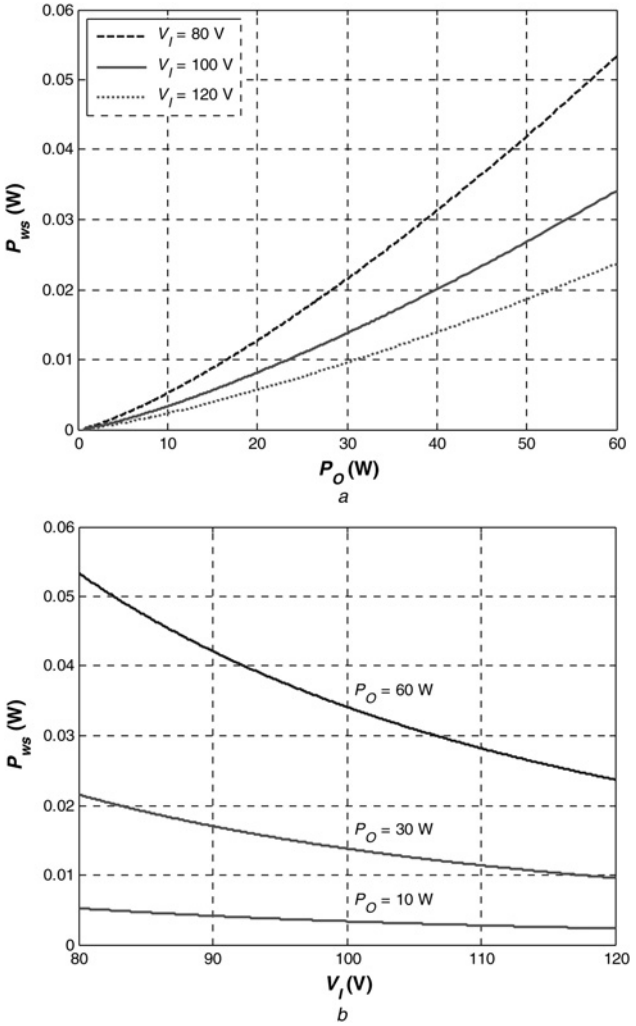

Figure 4 *Secondary winding loss*

a Secondary winding loss P_{ws} as a function of the output power P_O at fixed values of the dc input voltage V_I

b Secondary winding loss P_{ws} as a function of the dc input voltage V_I at fixed values of the output power P_O

doi: 10.1049/iet-pel.2009.0289

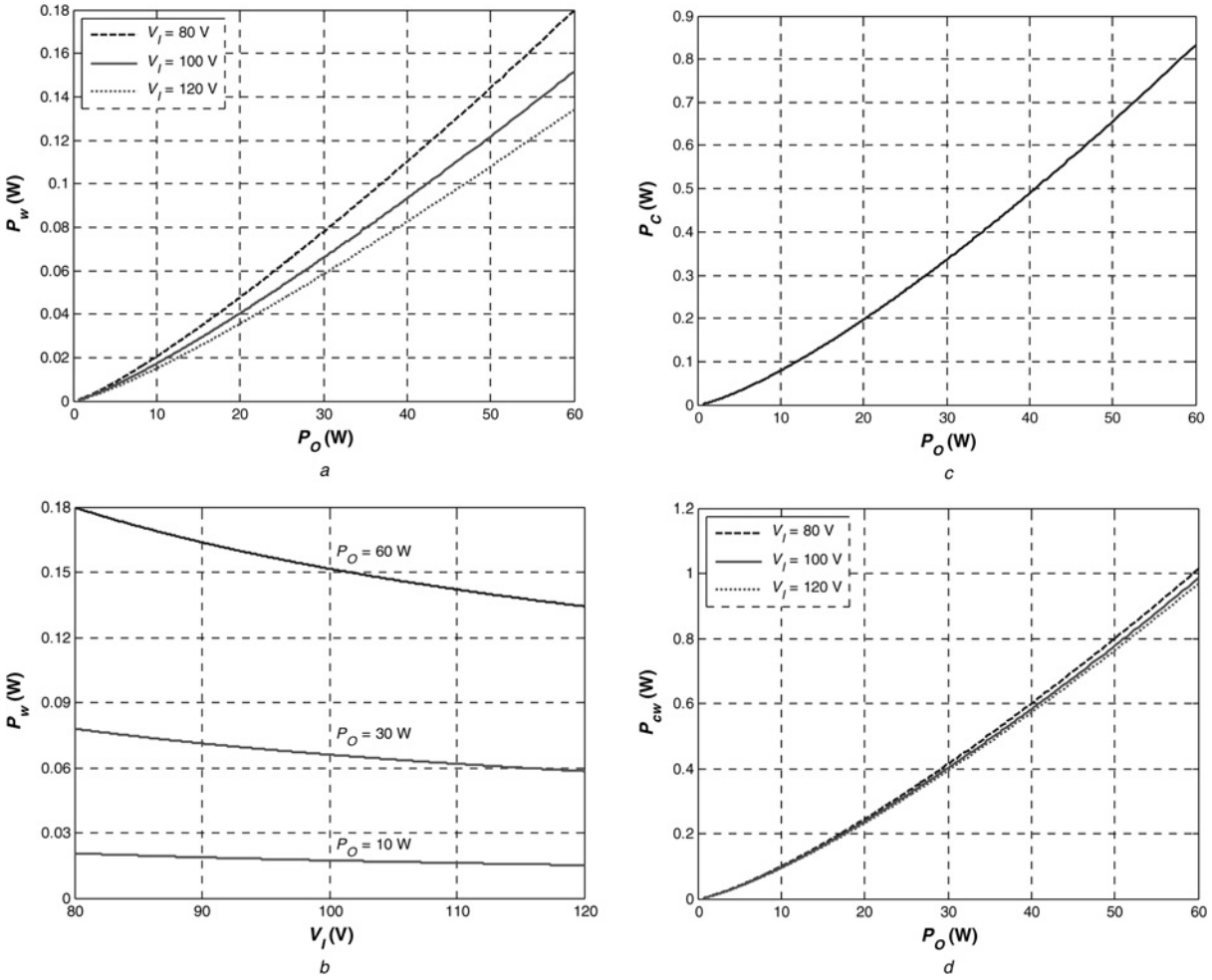

Figure 5 *Transformer power losses*

a Primary and secondary winding loss P_w as a function of the output power P_O at fixed values of the dc input voltage V_I
b Primary and secondary winding loss P_w as a function of the dc input voltage V_I at fixed values of the output power P_O
c Core loss P_C as a function of the output power P_O
d Total transformer power loss P_{cw} as a function of the output power P_O at fixed values of the dc input voltage V_I

Similarly, using the effective secondary winding resistance R_{wse}, the effective secondary winding resistance factor is

$$K_{Rsh} = \frac{R_{wse}}{R_{wsdc}} = \frac{1 + (1/2)\sum_{n=1}^{\infty} F_{Rsn}(I_{sn}/I_{sdc})^2}{1 + (1/2)\sum_{n=1}^{\infty} (I_{sn}/I_{sdc})^2}$$

$$= \frac{F_{Rsh}}{1 + (1/2)\sum_{n=1}^{\infty} (I_{sn}/I_{sdc})^2} \quad (31)$$

resulting in the total secondary winding power loss

$$P_{ws} = R_{wse} I_{s(rms)}^2 = K_{Rsh} R_{wsdc} I_{s(rms)}^2 \quad (32)$$

4 HF flyback transformer design for DCM

The above theory will be illustrated by the case study of the transformer used in the flyback converter operating in DCM. The following specifications of the flyback converter are used: dc input voltage $V_I = 100 \pm 20$ V, dc output voltage $V_O = 48$ V, maximum output power $P_O = 60$ W, and switching frequency $f_s = 100$ kHz. Using the procedure for the flyback converter design [34], a step-by-step design procedure of the transformer is given in Table 1.

5 Characteristics of HF transformer for flyback converter in DCM

In this section, the computed characteristics of the designed transformer are presented for a wide range of operating conditions of the flyback converter in DCM, that is, over the entire range of the load current and the dc input voltage. Plots of primary winding harmonic loss factor F_{Rph} as functions of output power and input voltage are shown in Figs. 2*a* and *b*, respectively, using (14), (20) and (15) for $N_l = 2$, $d/\delta_{w1} = 1.9378$, $d/p = 0.8$ and $n = 100$. Plot of secondary winding harmonic loss factor F_{Rsh} as a function of output power is shown in Fig. 2*c*, using (14), (20) and (27) for $N_l = 1$, $d/\delta_{w1} = 1.9378$, $d/p = 0.8$ and $n = 100$. Table 2

gives the variation of F_{Rph} and F_{Rsh} with respect to the number of harmonics n at full power and maximum dc input voltage. The values of F_{Rph} and F_{Rsh} were calculated with $n = 100$ for all the plots. When $D + D_1$ is close to 1, a lower number of harmonics n is sufficient, typically $n = 50$. When $D + D_1$ is low, then higher number of harmonics is needed, typically $n = 100$. From Fig. 2, it is clearly seen that the maximum values of F_{Rph} and F_{Rsh} occur at light load and maximum input voltage. This is because at light load, the duty cycle is low and the primary/secondary winding current contains many significant harmonics. The values of F_{Rph} and F_{Rsh} at full load and maximum input voltage for a specific case of the DCM flyback transformer are predicted to be about 23 and 5, respectively. Plots of effective primary and secondary resistance factors K_{Rph} and K_{Rsh} are shown in Figs. 2*d* and *e*, respectively, for $n = 100$. The values of K_{Rph} and K_{Rsh} at full load and maximum input voltage for a specific case of the DCM flyback transformer are predicted to be about 5 and 1.6, respectively. As the output power P_O

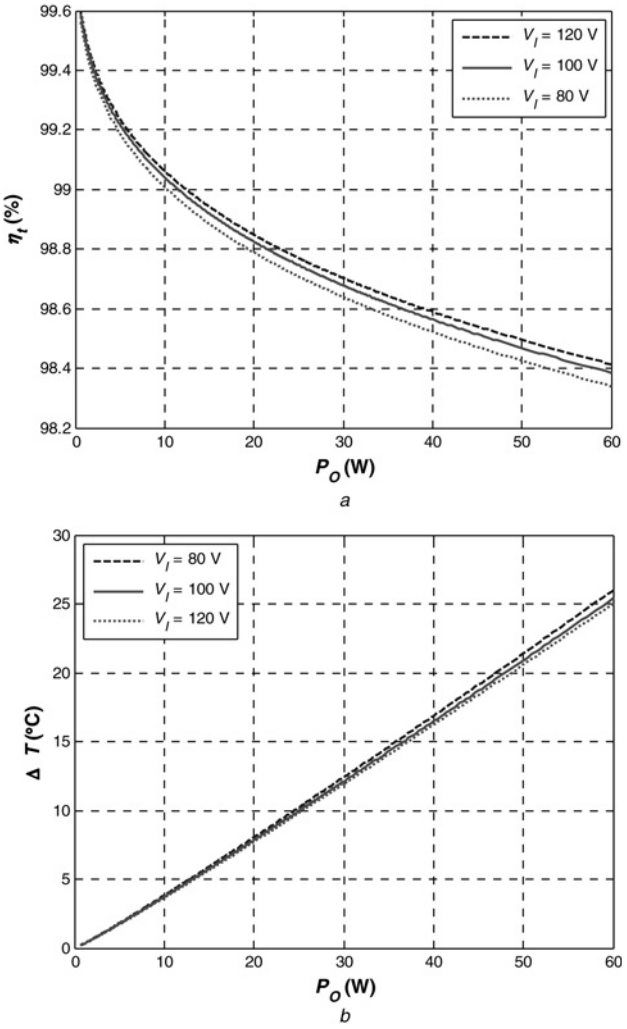

Figure 6 *Transformer efficiency and temperature rise*

a Transformer efficiency of the flyback converter in DCM as a function of the output power P_O at fixed values of the dc input voltage V_I

b Flyback transformer temperature rise as a function of the output power P_O at fixed values of the dc input voltage V_I

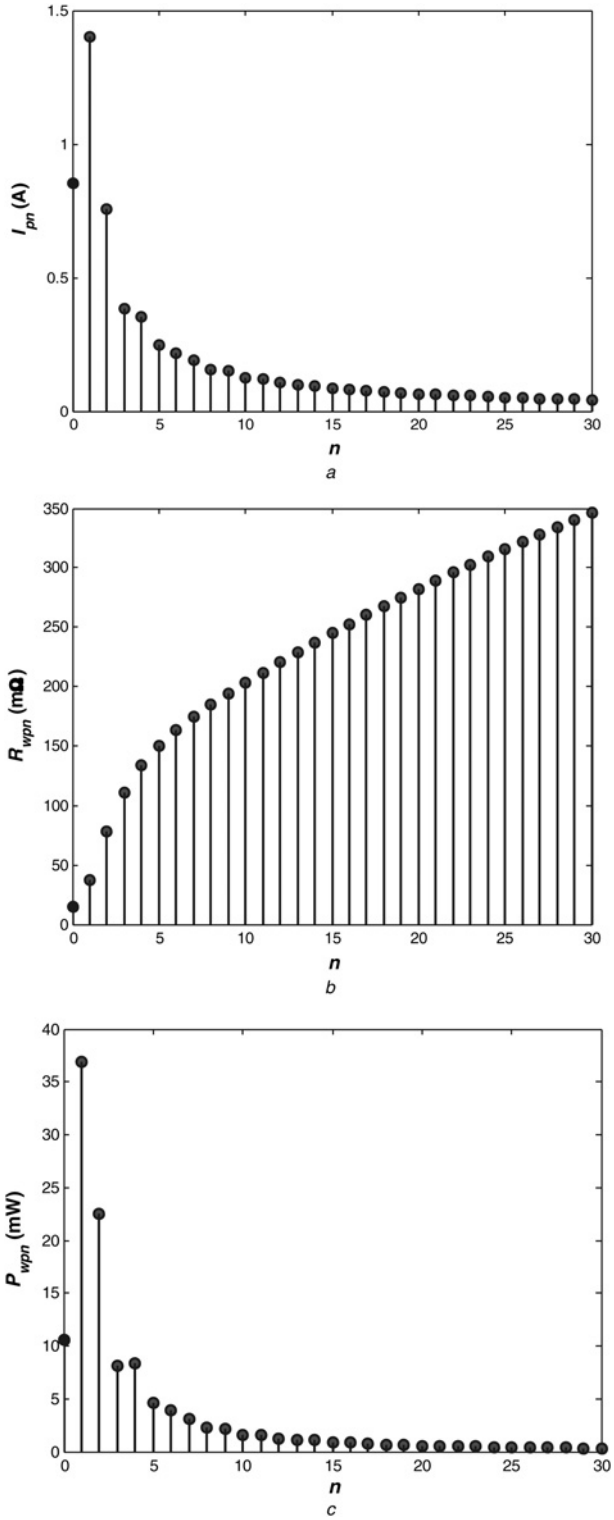

Figure 7 *Spectrum of primary current, winding resistances and winding power losses at minimum dc input voltage and maximum output power*

a The amplitudes of the fundamental component and the harmonics of the flyback transformer primary winding current at minimum dc input voltage and maximum output power

b Spectrum of the primary winding ac resistance of the flyback transformer

c Spectrum of the primary winding power loss of the flyback transformer at minimum dc input voltage and maximum output power

doi: 10.1049/iet-pel.2009.0289

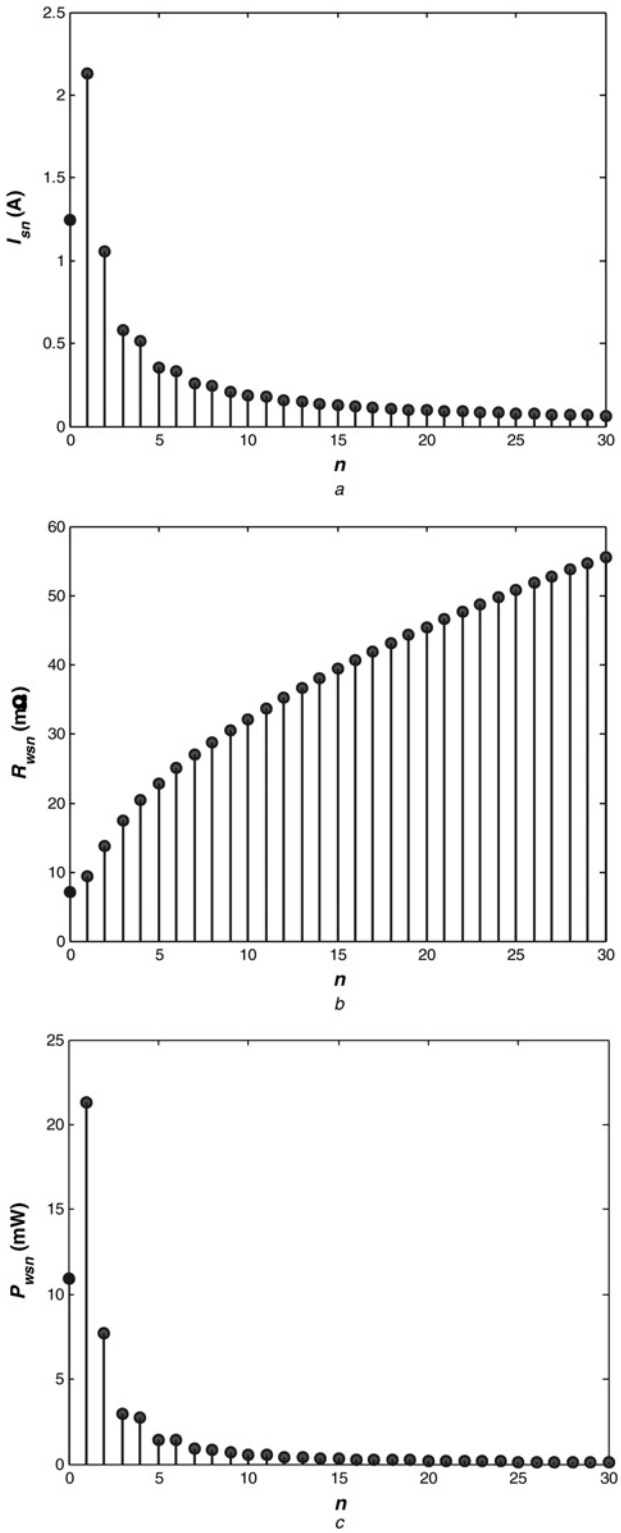

Figure 8 *Spectrum of secondary current, winding resistances and winding power losses at minimum dc input voltage and maximum output power*

a The amplitudes of the fundamental component and the harmonics of the flyback transformer secondary winding current at minimum dc input voltage and maximum output power

b Spectrum of the secondary winding ac resistance of the flyback transformer

c Spectrum of the secondary winding power loss of the flyback transformer at minimum dc input voltage and maximum output power

decreases, both K_{Rph} and K_{Rsh} increase because of the decrease in the duty cycle. Using F_{Rph} and the primary winding dc power loss, the plots of primary winding loss as a function output power at fixed values of input voltage and as a function of input voltage at fixed values of output power, are shown in Figs. 3*a* and *b*, respectively. The maximum primary winding power loss occurs at full load and minimum input voltage. Using F_{Rsh} and the secondary winding dc power loss, the plots of secondary winding loss as a function of output power at fixed values of input voltage and as a function of input voltage at fixed values of output power, are shown in Figs. 4*a* and *b*, respectively. The maximum secondary winding power loss occurs at full load and minimum input voltage.

The plots of total winding power loss of the transformer as a function of output power at fixed values of input voltage and as a function of input voltage at fixed values of output power, are shown in Figs. 5*a* and *b*, respectively. The maximum total winding power loss occurs at full load and minimum input voltage. The plot of core loss as a function of output power is shown in Fig. 5*c*. The core loss is calculated using steps 13, 29 and 41–44 in Table 1. The plot of total power loss of the transformer as a function of output power at fixed values of input voltage is shown in Fig. 5*d*. The maximum total power loss of the transformer occurs at full load and minimum input voltage. Fig. 6*a* shows the efficiency of the transformer as a function of output power. As expected, the minimum efficiency of the transformer occurs at full load and minimum input voltage. Fig. 6*b* shows the temperature rise in the flyback transformer as a function of output power at fixed values of input voltages. Figs. 7*a*–*c* show the spectrum of the primary winding current, the primary winding ac resistance, and the primary winding power loss, respectively, for the flyback transformer in DCM at full load and minimum input voltage. The ac resistances of the primary winding of the transformer measured at 100, 200 and 400 kHz were 35.1, 76.8 and 138 mΩ, respectively, and were in excellent agreement with the theoretical values presented in Fig. 7*b*. Figs. 8*a*–*c* show the spectrum of the secondary winding current, the secondary winding ac resistance, and the secondary winding power loss, respectively, for the flyback transformer in DCM at full load and minimum input voltage. The ac resistances of the secondary winding of the transformer measured at 100, 200 and 400 kHz were 15.48, 28.22 and 494.7 mΩ, respectively, and were in fairly good agreement with the theoretical values presented in Fig. 8*b*. The winding ac resistances were measured using Hewlett Packard 4275A multi-frequency LCR meter.

6 Conclusions

Expressions for the winding power loss for transformer primary and secondary periodic non-sinusoidal triangular current waveforms have been derived. Dowell's theory developed for sinusoidal currents in magnetic devices has been used for multi-harmonic waveforms. Fourier expansion of transformer triangular current waveforms for

any duty cycle has been derived for single-ended isolated dc–dc converters operated in DCM. A case study for copper losses in a flyback PWM converter operating in DCM has been presented. The maximum transformer temperature rise has been estimated.

For DCM operation of PWM converters, the winding power loss because of harmonics of the transformer currents is not negligible. The number of significant harmonics in PWM converters operating in DCM is high, of the order of 50–100. As the duty cycle decreases, the number of significant harmonics increases. The power losses in both windings change when the dc input voltage and the load current of the converter is varied. The maximum winding power loss occurs at full load and minimum dc input voltage for the flyback converter. The primary winding harmonic loss factor F_{Rph} and the secondary winding harmonic loss factor F_{Rsh} significantly increase as $D + D_1$ decreases, both of which occur when the output power decreases. The effective primary resistance factor K_{Rph} and the effective secondary resistance factor K_{Rsh} also significantly increase as $D + D_1$ decreases. The core loss of the transformer increases with increasing output power. In the example given in this paper, the core loss was higher than the winding loss. The estimated temperature rise of the transformer was 26°C. The theory presented in this paper can be used to design transformers for other isolated PWM dc–dc converters as well as transformers used in DC-AC inverters with non-sinusoidal transformer current waveforms.

7 References

[1] TAN G.H., WANG J.Z., JI Y.C.: 'Soft-switching flyback inverter with enhanced power decoupling for photovoltaic applications', *IET Proc. Electr. Power Appl.*, 2007, **1**, (2), pp. 264–274

[2] LAI C.M., SHYU K.K.: 'A single-stage AC/DC converter based on zero voltage switching LLC resonant topology', *IET Proc. Electr. Power Appl.*, 2007, **1**, (5), pp. 743–752

[3] WAI R.J., LIN C.Y., LIU L.W., CHANG Y.R.: 'High efficiency single-stage bidirectional with multiple-input power sources', *IET Proc. Electr. Power Appl.*, 2007, **1**, (5), pp. 763–777

[4] LIN B.R., HUANG C.L., LI M.Y.: 'Novel zero voltage switching dual-switch forward converter with ripple current cancellation', *IET Proc. Electr. Power Appl.*, 2007, **1**, (5), pp. 799–807

[5] LIN B.R., HUANG C.L.: 'Zero voltage switching active clamp buck-boost stage Cuk converter', *IET Proc. Electr. Power Appl.*, 2007, **1**, (2), pp. 173–182

[6] BENNETT E., LARSON S.C.: 'Effective resistance to alternating currents of multilayer windings', *Trans. AIEE*, 1940, **59**, pp. 1010–1016

[7] DOWELL P.L.: 'Effect of eddy currents in transformer windings', *IEE Proc.*, 1966, **113**, (8), pp. 1387–1394

[8] PERRY M.P.: 'Multiple layer series connected winding design for minimum losses', *IEEE Trans. Power Appar. Syst.*, 1979, **98**, (1), pp. 116–123

[9] VENKATRAMAN P.S.: 'Winding eddy current losses in switch mode power transformers due to rectangular wave currents'. Proc. Powercon 11, Section A-1, 1984, pp. 1–11

[10] CARSTEN B.: 'High frequency conductor losses in switchmode magnetics'. Proc. HPFC, pp. 155–176

[11] JONGSMA J.: 'Minimum loss transformer windings for ultrasonic frequencies – Part 3: transformer winding design', *Phillips Electron. Appl. Bull.*, 1978, **E.A.B.**, (35), pp. 211–226

[12] JONGSMA J.: 'High-frequency ferrite power transformer and choke design – Part 3: transformer winding design', *Phillips Electron.-Comp. Mater. Tech.*, 1986, (207), pp. 1–28

[13] VANDELAC J., ZIOGAS P.D.: 'A novel approach for minimizing high-frequency transformer copper losses', *IEEE Trans. Power Electron.*, 1988, **3**, (3), pp. 166–176

[14] ROSA J.: 'Calculation of flux linkages in multiwinding transformers'. IEEE Power Electronics Specialists Conf. Record, 1986, 86CH2310-1, pp. 639–644

[15] COONROD N.R.: 'Transformer computer design aid for higher frequency switching power supplies'. IEEE Power Electronics Specialists Conf. Record, 1984, 84CH2000-8, pp. 257–267

[16] HURLEY W.G., GATH E., BRESLIN J.G.: 'Optimizing the AC resistance of multilayer transformer windings with arbitrary current waveforms', *IEEE Trans. Power Electron.*, 2000, **15**, (2), pp. 369–376

[17] URLING A.M., NIEMELA V.A., SKUTT G.R., WILSON T.G.: 'Characterizing high-frequency effects in transformer windings – a guide to several significant articles'. IEEE APEC, March 1989, pp. 373–385

[18] KASSAKIAN J.G., SCHLECHT M.F.: 'High-frequency high-density converters for distributed power-supply systems', *Proc. IEEE*, 1988, **76**, pp. 362–376

[19] WILLIAMS R., GRANT D.A., GOWAR J.: 'Multielement transformers for switched-mode power-supplies: Toroidal designs', *IEE Proc.*, 1993, **140**, (2), pp. 152–160

[20] CHENG K.W.E., EVANS P.D.: 'Calculation of winding losses in high-frequency toroidal inductors using multistrand conductors', *IEE Proc. Electric Power Appl.*, 1995, **142**, (5), pp. 313–322

doi: 10.1049/iet-pel.2009.0289

[21] CHENG K.W.E., EVANS P.D.: 'Calculation of winding losses in high-frequency toroidal inductors using single strand conductors', *IEE Proc. Electric Power Appl.*, 1994, **141**, (2), pp. 52–62

[22] EVANS P.D., CHEW W.M.: 'Reduction of proximity losses in coupled inductors', *Proc. Inst. Elect. Eng. B*, 1991, **138**, (2), pp. 51–58

[23] HANSELMAN D.C., PEAKE W.H.: 'Eddy-current effects in slot-bound conductors', *Proc. Inst. Elect. Eng. B – Electr. Power Appl.*, 1995, **142**, pp. 131–136

[24] HURLEY W.G., WÖLFLE W., BRESLIN J.G.: 'Optimized transformer design: Inclusive of high frequency effects', *IEEE Trans. Power Electron.*, 1998, **13**, (4), pp. 651–659

[25] PETKOV R.: 'Optimized design of a high-power high-frequency transformer', *IEEE Trans. Power Electron.*, 1996, **11**, (1), pp. 33–42

[26] BARTOLI M., REATTI A., KAZIMIERCZUK M.K.: 'Modeling iron-powder inductors at high-frequencies'. IEEE Proc. Ind. Appl. Society Annual Meeting, Denver, USA, October 1994, pp. 1225–1232

[27] BARTOLI M., NOFERI N., REATTI A., KAZIMIERCZUK M.K.: 'Modeling winding losses in high-frequency power inductors', *J. Circuits, Syst. Comput.*, 1995, **5**, (4), pp. 607–626

[28] BARTOLI M., NOFERI N., REATTI A., KAZIMIERCZUK M.K.: 'Modeling litz-wire winding losses in high-frequency power inductors'. IEEE Power Electronics Specialists Conf. Record, 1996, pp. 1690–1696

[29] GRANDI G., KAZIMIERCZUK M.K., MASSARINI A., REGGIANI U., SANCINETO G.: 'Model of laminated iron-core inductors', *IEEE Trans. Magn.*, 2004, **40**, (4), pp. 1839–1845

[30] MURTHY-BELLUR D., KAZIMIERZCUK M.K.: 'Harmonic winding loss in buck DC-DC converter for discontinuous conduction mode', *IET Power Electron.*, 2010, **3**, (in press)

[31] KAZIMIERCZUK M.K., SEKIYA H.: 'Design of ac resonant inductors using area product method'. Proc. First Energy Conversion Conf. and Expo, San Jose, USA, September 2009, pp. 994–1001

[32] SEKIYA H., KAZIMIERCZUK M.K.: 'Design of RF-choke inductors using core geometry coefficient'. Proc. Electrical Manufacturing and Coil Winding Conf., Nashville, USA, September 29–October 1, 2009

[33] MCLYMAN W.T.: 'Transformer and inductor design handbook' (Marcel Dekker, 2004, 3rd edn.)

[34] KAZIMIERCZUK M.K.: 'Pulse-width modulted DC-DC power converters' (John Wiley & Sons, 2008)